

Phase separation induces congestion waves in electric vehicle chargingPhilip Marszal ¹, Marc Timme ^{1,2,3} and Malte Schröder ¹¹*Chair for Network Dynamics, Center for Advancing Electronics Dresden (cfaed) and Institute for Theoretical Physics, Technical University of Dresden, 01062 Dresden, Germany*²*Cluster of Excellence Physics of Life, Technical University of Dresden, 01062 Dresden, Germany*³*Lakeside Labs, Lakeside B04b, 9020 Klagenfurt, Austria*

(Received 4 May 2021; accepted 24 September 2021; published 26 October 2021)

Electric vehicles may dominate motorized transport in the next decade, yet the impact of the collective dynamics of electric mobility on long-range traffic flow is still largely unknown. We demonstrate a type of congestion that arises if charging infrastructure is limited or electric vehicle density is high. This congestion emerges solely through indirect interactions at charging infrastructure by queue-avoidance behavior that—counterintuitively—induces clustering of occupied charging stations and phase separation of the flow into free and congested stations. The resulting congestion waves always propagate forward in the direction of travel, in contrast to typically backward-propagating congestion waves known from traditional traffic jams. These results may guide the planning and design of charging infrastructure and decision support applications in the near future.

DOI: [10.1103/PhysRevE.104.L042302](https://doi.org/10.1103/PhysRevE.104.L042302)

The ongoing transition towards more sustainable mobility centrally relies on electric vehicles to provide low-emission transport. As the number of battery electric vehicles (EVs) grows rapidly [1–3], EVs may soon become the primary form of individual mobility [4]. However, with their limited range and long recharge periods, EVs critically depend on the available charging infrastructure.

Current research on electric mobility thus focuses on cornerstone aspects surrounding the charging process, including the technical implementation of charging and battery technologies [5,6], the optimal placement of charging infrastructure [7–12], and the efficient routing of vehicles within a given infrastructure [13,14]. In addition, the dependence of electric vehicles on the charging infrastructure has prompted investigations of the interactions, risks, and potential synergies between electric mobility and the larger-scale power grids and energy infrastructure [15–17]. Yet, fundamental aspects of the collective EV charging dynamics remain poorly understood to date.

In the past, researchers have applied methods of statistical physics, nonlinear dynamics, network science, and complex systems theory to the dynamics of traffic and mobility systems with astounding success. Applications range from describing congestion and phase coexistence in traffic flow and transport processes [18–23] to understanding the complex interactions in modern networked mobility systems [24–31].

In this Letter, we study the collective dynamics of electric vehicles and their interaction with charging infrastructure. We uncover a class of spatiotemporal congestion states for long-distance travel. In particular, we find congestion waves that are caused solely by indirect interactions of the vehicles with the charging infrastructure in the form of queueing dynamics. We explain the emergence of these waves through phase separation of the charging demand along the available infrastructure.

Interestingly, the congestion waves always propagate in the direction of travel, not against it as known for typical [32,33] congestion waves in traditional traffic flow.

Electric vehicle travel differs from travel by internal combustion engine (ICE) vehicles in two key aspects. Firstly, current EVs possess a typical range of the order of 300 km [34], significantly lower than that of ICE vehicles. Secondly, EVs recover range slowly during charging. A recharging event at a fast charging station typically lasts more than 20 min [35] and even high-end EVs need about 30 min to recharge 80% of their battery [36]. As an example of a characteristic EV recharging rate, we consider $\xi = 480$ km/h. In contrast, internal combustion engine vehicles take mere minutes to refuel, with refuelling rates $\xi_{\text{ICE}} > 10^4$ km/h. Consequently, refueling times contribute little to average ICE vehicle travel times while recharging times contribute substantially to EV travel times on long-distance trips.

Electric vehicles traveling over long distances s spend characteristic times $t_{\text{driving}} = s/v$ moving and $t_{\text{charging}} = s/\xi$ charging. Their average velocity

$$v_F = \frac{s}{t_{\text{driving}} + t_{\text{charging}}} = \frac{1}{1/v + 1/\xi} \quad (1)$$

is thus only partly determined by the characteristic driving velocity v . For instance, for $v = 120$ km/h, the charging time contribution to travel time yields an effective velocity of $v_F = 96$ km/h, representing a decrease of 20% due to charging alone. Queues at charging stations exacerbate this effect because waiting times add to the charging times and further reduce the effective velocity. Faced with waiting times comparable in length to the travel time, EV drivers are likely to employ strategies to avoid queues, similar to queue avoidance behavior observed, for example, during shopping [37] and parking [38].

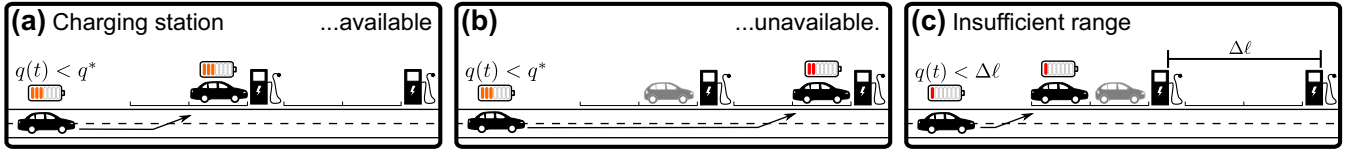


FIG. 1. Charging decisions of EVs. At each charging station, vehicles decide to charge or to continue driving. (a) If the remaining range is smaller than a threshold, $q(t) \leq q^*$, the EV charges at an available charging station without a queue. (b) If the charging station is currently unavailable and the range is sufficient to reach the next station down the road, the vehicle continues driving to avoid the queue. (c) If the vehicles range is insufficient to reach the next charging station, $q(t) < \Delta\ell$, it charges at its current station regardless of queue length.

We consider the basic dynamics of an EV battery gaining and losing charge, specified in terms of the range $q(t)$ available to the vehicle at time t . A fully charged vehicle has a maximum range q_{\max} . While driving with a fixed velocity v , the available range decreases linearly with time.

At each charging station, the vehicle decides to charge or to continue driving (Fig. 1). If the available range is below a threshold, $q(t) \leq q^*$, and the charging station is available, the vehicle stops to charge. If there is a queue at the charging station and the vehicle has sufficient range to reach the next station, it continues driving to avoid the queue. If at any time the vehicle does not have sufficient range $q(t) < \Delta\ell$ to reach the next charging station at distance $\Delta\ell$, it charges at its current station regardless of the queue length to avoid running out of range in the middle of the road. During the charging process, the vehicle regains range at a constant rate ξ until it is fully charged and continues driving.

To isolate the impact of the charging process on electric vehicle travel, we analyze a basic model where vehicles do not interact or contribute to congestion while driving between charging stations. We focus on a highwaylike system with total length L and periodic boundaries with K equidistant charging stations, each with m charging ports, separated by a distance $\Delta\ell = L/K$. Vehicles enter the system at a uniformly random charging station following a Poisson process with rate λ with a uniformly sampled random initial charge $q(0) \in [0, q_{\max}]$. They travel an average distance $L/2$ and exit the system at another uniformly random charging station. Thus, to complete their journey, a fraction of vehicles will need to recharge at least once.

At a critical rate

$$\lambda_c = \frac{2mK\xi}{L}, \quad (2)$$

the average consumed range per unit time $\lambda L/2$ exactly matches the maximum total range $mK\xi$ potentially supplied by all charging stations per unit time. For $\lambda \ll \lambda_c$, the system is in *free flow* with vehicles traveling with an average velocity v_F , unaffected by charging queues [Fig. 2(a)]. While short queues may appear randomly even at low numbers of vehicles, they dissolve quickly as vehicles do not enter any particular queue consistently. In contrast, for $\lambda > \lambda_c$, the charging infrastructure cannot supply sufficient range for all vehicles. On average, queues grow at every charging station and the system is *overloaded* [Fig. 2(b)]. A third, qualitatively different state emerges at rates just below the critical rate λ_c where self-organized *congestion waves* form across the charging stations [Fig. 2(c)]. Like in conventional traffic jams, regions of high vehicle density, here represented by long queue lengths at

some charging stations, restrict the flow of vehicles. When queues emerge at localized groups of stations, they propagate along the system with a velocity substantially lower than the effective velocities of the vehicles [slopes of dashed vs purple lines in Fig. 2(c)].

In contrast to conventional traffic jams that often propagate backwards, against the direction of travel, charging congestion waves always propagate in the direction of travel. Conventional traffic jams grow at the upstream boundary due to the inability of vehicles to pass through each other on the road, forcing cars to stop or slow down when reaching the traffic jam. In contrast, charging congestion is caused solely by the queue avoidance and charging processes of the vehicles. Vehicles that encounter a group of occupied charging stations continue driving to recharge further downstream due to their reluctance to enqueue. Once the vehicles are forced

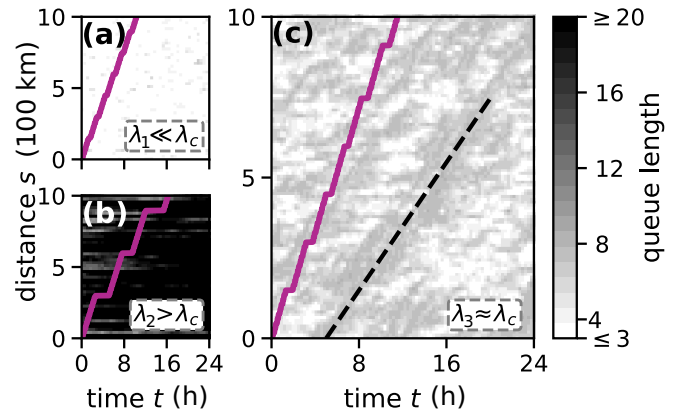


FIG. 2. Three classes of collective EV charging dynamics. Space-time plots show the number of vehicles (increasing from white to black) at charging stations distributed along a simulated circular highway with a theoretical capacity λ_c (see main text). (a) At low inflow rates (few EVs entering the highway per time, $\lambda_1 \ll \lambda_c$), only short, transient queues appear. The trajectory (purple line) of a single vehicle is characterized by frequent, short charging stops moving with an effective velocity given by Eq. (1). (b) At $\lambda_2 > \lambda_c$, the system becomes overloaded as vehicles spend a significant amount of time waiting at a charging station; the sample trajectory (purple) exhibits long waiting periods (horizontal) and a significantly smaller effective velocity (average slope). (c) A third regime emerges at intermediate inflow rates ($\lambda_3 \approx \lambda_c$), exhibiting persistent short queues at some charging stations (gray) that propagate forward in the form of waves (dashed line) at a velocity substantially lower than vehicle velocity (purple). The congested state emerges already at $\lambda_3 < \lambda_c$. Model settings in main text; see [1] and [39] for additional details.

to enqueue as their remaining charge is too low to reach the next station, they enter queues in the bulk or at the downstream end of the jam. Simultaneously, queues at the upstream end shrink as more vehicles finish charging than enter that queue. Thus, queue lengths grow downstream of the jam and shrink upstream, thereby causing a forward-propagating wave of occupied charging stations. This mechanism is similar to forward-propagating conventional traffic jams where traffic does not come to a complete standstill in the regions of high vehicle density, moving the congestion forward with it [32,40]. Similarly, the electric vehicles in our model still drive in the jammed region though with a lower effective velocity due to charging queues. These dynamics remain robust under substantially more general conditions such as heterogeneous properties of both vehicles and charging stations, including varying charging rates, vehicle velocities, maximum ranges, number of ports per station, and station locations (see Supplemental Material [1]).

We observe the congestion waves more clearly if the total number and thus the overall density of vehicles ρ on the highway is conserved. To estimate the maximum density ρ_c of vehicles at which a free-flow state is possible, we consider vehicles as sinks of total charge, i.e., range, available in the system and charging stations as sources. Jointly, all K charging stations maximally provide new range $mK\xi$ per unit time. Under free-flow conditions, each vehicle consumes charge at a rate matching the effective velocity v_F defined in Eq. (1), in total consuming a range of $L\rho v_F$. Balancing these source and sink strengths and substituting $K = L/\Delta\ell$ yields the critical density

$$\rho_c = \frac{m\xi}{v_F\Delta\ell} \quad (3)$$

of vehicles on the highway.

The fundamental diagram (Fig. 3) that links the flow $Q(\rho) = v(\rho)\rho$ to the vehicle density, offers two helpful relations for quantifying the properties of traffic flow [32]. First, it provides the time-average velocity

$$\langle v \rangle = \frac{\langle Q(\rho) \rangle}{\rho} \quad (4)$$

of the vehicles. Second, it offers insights about the propagation of density variations of the form $\bar{\rho}(x - ct)$ through the group velocity [32]

$$c = \frac{\partial \langle Q(\rho) \rangle}{\partial \rho}. \quad (5)$$

At densities $\rho < \rho_c$, queues do not form at all. In this free-flow state, the average velocity is independent of the vehicle density and the flow increases linearly with the number of vehicles in the system. Without queue avoiding behavior [$q^* = 0$; Fig. 3(b)], the system overloads as the density exceeds the critical density ρ_c , where the flow saturates and becomes density independent, $\langle Q(\rho) \rangle = \xi/\Delta\ell$, because it is limited by the total available charging rate. Furthermore, since the group velocity $c = 0$, density fluctuations do not propagate in space and the vehicle densities at all charging stations are approximately constant in time [compare Fig. 2(b)].

With active queue avoidance, $q^* > 0$ [Figs. 3(c) and 3(d)], the flow dynamic changes fundamentally. Close to the critical

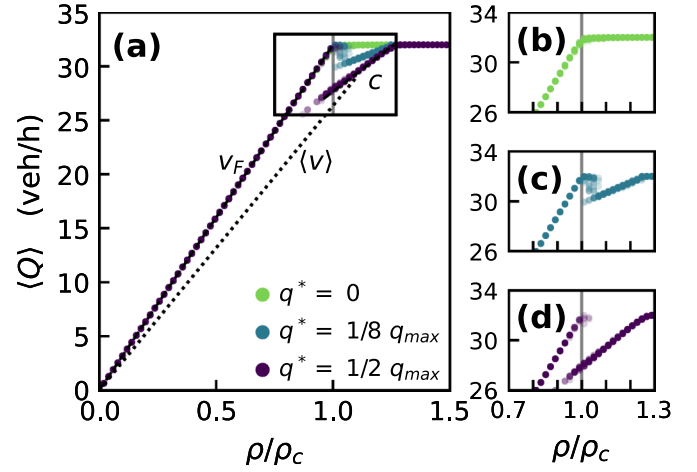


FIG. 3. Congestion waves near the critical density. (a) The fundamental diagram quantifies the flow states as a function of the vehicle density qualitatively observed in Fig. 2. At low densities the system settles in a free-flow state where $\langle Q \rangle = v_F \rho$, with an effective velocity v_F defined by Eq. (1). Substantially above the critical density, the system overloads and the flow saturates at a maximum flow $\langle Q \rangle = Q_{\max}$ set by the total charging rate of the system. At intermediate densities $\rho/\rho_c \approx 1$, a congested state emerges, reducing the average velocity of individual vehicles to $\langle v \rangle = \langle Q \rangle / \rho$. Congestion waves move at a group velocity $c = \partial \langle Q \rangle / \partial \rho > 0$ indicated by the local slope. (b) The congested state does not emerge if vehicles deplete their batteries completely before charging [$q^* = 0$ (light green)]. (c),(d) Congestion occurs at lower densities for higher charging thresholds [(c), $q^* = 1/8 q_{\max}$ (blue) and (d) $q^* = 1/2 q_{\max}$ (purple)]. The fundamental diagram shows the time-averaged flow from 25 realizations for each density in a system with a fixed number of vehicles $N = \rho L$ and $m = 1$ charging port per station; all other parameters are identical to Fig. 2.

density ρ_c , the fundamental diagram exhibits a discontinuity and propagating congestion waves emerge, decreasing the flow regardless of whether the system would be overloaded or in free flow. The discontinuity becomes stronger with larger charging threshold and the flow exhibits bistability: congestion waves may already emerge at densities below ρ_c , effectively decreasing the critical density before the free-flow state breaks down.

To further understand the spatiotemporal structure of the congestion waves, we classify each station as either congested or free at a given time, taking into account the immediate temporal and spatial neighborhood using a Gaussian mixture model [Fig. 4(a); see [1] for details]. The probability density for finding a certain vehicle density at a station differs between the congested and the free-flow state. The probability densities exhibit peaks below the critical vehicle density ρ_c in the free-flow state and above ρ_c in the congested state.

These findings indicate the emergence of phase separation in the system. In a system exhibiting congestion waves at some density ρ_0 close to ρ_c , the flow splits into two distinct phases of flow, represented by two points on the fundamental diagram. As observed in Fig. 4(a), the free-flow phase has an average conditional vehicle density $\rho_{\text{free}} < \rho_c$, the congested flow phase has an average conditional density $\rho_{\text{jam}} > \rho_c$, both insensitive to the total vehicle density ρ_0 (see [1]). These flow

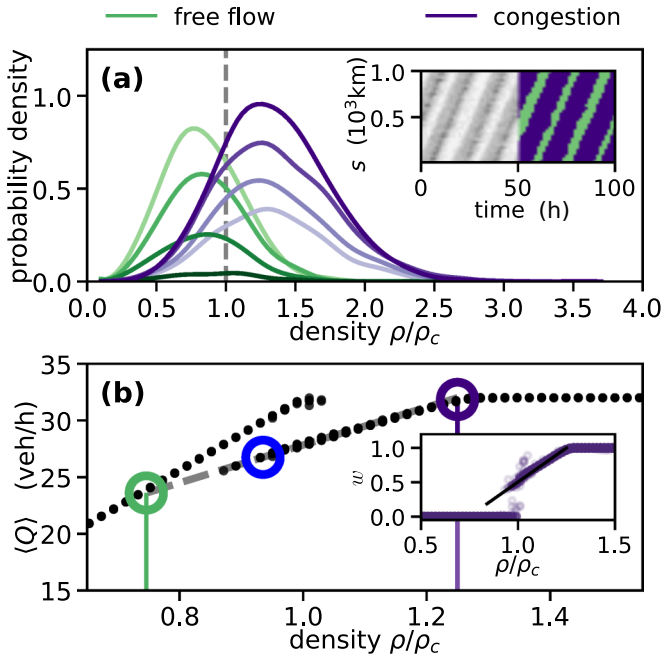


FIG. 4. Phase separation of the flow into a free-flow phase and an overloaded phase. (a) Continuous interpolation of the conditional probability distributions of the vehicle densities in both states. The system separates into a free-flow state with low density (green) and an overloaded state with high density (purple). A larger overall vehicle density (darker colored lines) leads to a larger number of charging stations that are simultaneously congested captured in the relative weight of the probability density distributions. The average conditional densities of the respective free-flow and congested states, however, are independent of the overall density (see [1]). (a), inset: Classification into free-flow and congested states (see [1] for details). (b) Illustration of the phase separation along the tangent in the fundamental diagram. The flow of a system exhibiting propagating congestion at overall vehicle density ρ_0 is the weighted average of the flow in the congested phase (purple circle) and the flow in the free-flow phase (green circle). (b), inset: Measuring the conditional vehicle densities ρ_{free} in free-flow regions and ρ_{jam} in congested regions predicts the fraction w of congested stations using Eq. (6). The fraction of congested stations observed (points) matches the prediction (dashed line). Parameters are identical to Fig. 3 with charging threshold $q_c = 1/2 q_{\text{max}}$.

states are marked by the intersection of the tangent of the fundamental diagram at the point $(\rho_0, \langle Q(\rho_0) \rangle)$ with the free-flow and overloaded branch, respectively [Fig. 4(b)]. Since the conditional densities in the free-flow and congested phase are constant, the fraction w of congested stations is directly related to the overall vehicle density

$$\rho_0 = w\rho_{\text{jam}} + (1 - w)\rho_{\text{free}} \quad (6)$$

that is the weighted average of the free-flow and congested densities. Eq. (6) predicts the fraction of congested stations w just from the measured densities ρ_0 , ρ_{free} , and ρ_{jam} . Comparing the result to the measured fraction of congested stations

confirms this prediction and the phase separation hypothesis [see Fig. 4(b) inset].

In conclusion, our analysis demonstrates that charging dynamics of EVs together with individual queue-avoidance behavior jointly induce spatio-temporal congestion. Specifically, we find congestion waves of occupied charging stations without direct interactions of the vehicles on the road. These congestion waves always propagate forward, along the direction of travel as vehicles continue to drive past occupied charging stations and effectively enqueue at the downstream end of the jam. The phase separation into free-flow and overloaded stations underlying these congestion waves is similar to mechanisms of congestion phenomena in conventional traffic jams [32,41] and other transport processes [21,22] and to the phase separation known from standard thermodynamics such as the liquid-gas transition in van der Waals fluids [42], where the overall density is a superposition of the densities of one gas and one liquid phase. If charging infrastructure is limited or EV density is high, such congested states may further increase the overall travel time of EVs during long-distance trips, in addition to the already substantial charging times. Charging dynamics of EVs thus constitute an additional dimension in traffic flow analysis in addition to their impact on power systems [15–17], becoming increasingly relevant as society transitions toward electric transport.

The observed congestion states emerge exactly around the mean-field critical point, reflecting the economic equilibrium where charging stations are maximally utilized but the system is not yet overloaded. While high charging thresholds and vehicle densities strongly promote congestion, the congested states appear for a wide range of (heterogeneous) system parameters and conditions (see [1] for details). Understanding the dynamics of congestion waves in EV charging infrastructures in further detail for specific infrastructure scenarios may support civil engineers and policy makers to anticipate inefficiencies and implement countermeasures. Our results may already provide conceptual guidance on how to mitigate the problem of congestion waves in EV charging by highlighting the required information to design smart routing and charging suggestions [13,14]. Moreover, the insights illustrated above highlight one key ingredient to minimize the impact of charging congestion that goes beyond infrastructure development or technological progress: Decreasing the charging threshold, for example by strengthening confidence in the vehicle-predicted remaining range or by automating charging decisions, limits the congestion to a small range of vehicle densities.

More generally, our results indicate that emerging technologies not only change individual technical components underlying transport, such as vehicles or infrastructure. Given new forms of interactions among system elements, we also expect a range of unprecedented collective dynamics [30,43,44] emerging in future-compliant mobility systems we need to explore.

We thank Christopher Hecht for helpful discussions. M.T. acknowledges support from the German Research Foundation (Deutsche Forschungsgemeinschaft, DFG) through the Center for Advancing Electronics Dresden (cfaed).

- [1] See Supplemental Material at <http://link.aps.org/supplemental/10.1103/PhysRevE.104.L042302> for additional details on the model simulations, parameters, analysis methods, and robustness of the results, including Refs. [45–51].
- [2] International Energy Agency, Global electric car sales by key markets, 2010–2020, <https://www.iea.org/data-and-statistics/charts/global-electric-car-sales-by-key-markets-2015-2020>.
- [3] Kraftfahrtbundesamt, <https://www.kba.de>.
- [4] International Energy Agency, Global EV Outlook 2019, <https://www.iea.org/reports/global-ev-outlook-2019>.
- [5] Z. P. Cano, D. Banham, S. Ye, A. Hintennach, J. Lu, M. Fowler, and Z. Chen, Batteries and fuel cells for emerging electric vehicle markets, *Nat. Energy* **3**, 279 (2018).
- [6] R. Schmuch, R. Wagner, G. Hörpel, T. Placke, and M. Winter, Performance and cost of materials for lithium-based rechargeable automotive batteries, *Nat. Energy* **3**, 267 (2018).
- [7] M. Hardinghaus, M. Löcher, and J. E. Anderson, Real-world insights on public charging demand and infrastructure use from electric vehicles, *Environ. Res. Lett.* **15**, 104030 (2020).
- [8] A. Y. S. Lam, Y.-W. Leung, and X. Chu, Electric vehicle charging station placement: Formulation, complexity, and solutions, *IEEE Trans. Smart Grid* **5**, 2846 (2014).
- [9] Y. Xiong, J. Gan, B. An, C. Miao, and A. L. C. Bazzan, Optimal electric vehicle fast charging station placement based on game theoretical framework, *IEEE Trans. Intell. Transp. Syst.* **19**, 2493 (2017).
- [10] Y. Wang, J. Shi, R. Wang, Z. Liu, and L. Wang, Siting and sizing of fast charging stations in highway network with budget constraint, *Appl. Energy* **228**, 1255 (2018).
- [11] Y. He, K. M. Kockelman, and K. A. Perrine, Optimal locations of US fast charging stations for long-distance trip completion by battery electric vehicles, *J. Clean. Prod.* **214**, 452 (2019).
- [12] P. Jochem, E. Szimba, and M. Reuter-Oppermann, How many fast-charging stations do we need along European highways? *Transp. Res. Part D: Transp. Environ.* **73**, 120 (2019).
- [13] H. Qin and W. Zhang, Charging scheduling with minimal waiting in a network of electric vehicles and charging stations, in *Proceedings of the Eighth ACM international workshop on Vehicular Inter-Networking* (ACM, New York, USA, 2011), pp. 51–60.
- [14] F. Hausler, E. Crisostomi, A. Schlote, I. Radusch, and R. Shorten, Stochastic park-and-charge balancing for fully electric and plug-in hybrid vehicles, *IEEE Trans. Intell. Transp. Syst.* **15**, 895 (2013).
- [15] M. Wolinetz, J. Axsen, J. Peters, and C. Crawford, Simulating the value of electric-vehicle-grid integration using a behaviourally realistic model, *Nat. Energy* **3**, 132 (2018).
- [16] S. Morgenthaler, J. Dünzen, I. Stadler, and D. Withaut, Three stages in the co-transformation of the energy and mobility sectors, *Renew. Sustain. Energy Rev.* **150**, 111494 (2021).
- [17] Y. Xu, S. Çolak, E. C. Kara, S. J. Moura, and M. C. González, Planning for electric vehicle needs by coupling charging profiles with urban mobility, *Nat. Energy* **3**, 484 (2018).
- [18] P. I. Richards, Shock waves on the highway, *Oper. Res.* **4**, 42 (1956).
- [19] K. Nagel and M. Schreckenberg, A cellular automaton model for freeway traffic, *J. Phys. I* **2**, 2221 (1992).
- [20] B. S. Kerner, Three-phase traffic theory and highway capacity, *Physica A (Amsterdam, Neth.)* **333**, 379 (2004).
- [21] A. Parmeggiani, T. Franosch, and E. Frey, Phase Coexistence in Driven One-Dimensional Transport, *Phys. Rev. Lett.* **90**, 086601 (2003).
- [22] R. M. D’Souza, Coexisting phases and lattice dependence of a cellular automaton model for traffic flow, *Phys. Rev. E* **71**, 066112 (2005).
- [23] A. Loder, L. Ambühl, M. Menendez, and K. W. Axhausen, Understanding traffic capacity of urban networks, *Sci. Rep.* **9**, 16283 (2019).
- [24] A. Schadschneider, Statistical physics of traffic flow, *Physica A* **285**, 101 (2000).
- [25] T. Nagatani, The physics of traffic jams, *Rep. Prog. Phys.* **65**, 1331 (2002).
- [26] P. Santi, G. Resta, M. Szell, S. Sobolevsky, S. H. Strogatz, and C. Ratti, Quantifying the benefits of vehicle pooling with shareability networks, *Proc. Natl. Acad. Sci. USA* **111**, 13290 (2014).
- [27] M. M. Vazifeh, P. Santi, G. Resta, S. H. Strogatz, and C. Ratti, Addressing the minimum fleet problem in on-demand urban mobility, *Nature (London)* **557**, 534 (2018).
- [28] I. Karamouzas, B. Skinner, and S. J. Guy, Universal Power Law Governing Pedestrian Interactions, *Phys. Rev. Lett.* **113**, 238701 (2014).
- [29] N. Molkenthin, M. Schröder, and M. Timme, Scaling Laws of Collective Ride-Sharing Dynamics, *Phys. Rev. Lett.* **125**, 248302 (2020).
- [30] M. Schröder, D.-M. Storch, P. Marszal, and M. Timme, Anomalous supply shortages from dynamic pricing in on-demand mobility, *Nat. Commun.* **11**, 4831 (2020).
- [31] D.-M. Storch, M. Timme, and M. Schröder, Incentive-driven transition to high ride-sharing adoption, *Nat. Commun.* **12**, 3003 (2021).
- [32] M. Treiber and A. Kesting, *Traffic Flow Dynamics: Data, Models and Simulation* (Springer-Verlag, Berlin, Heidelberg, 2013).
- [33] B. S. Kerner and H. Rehborn, Experimental features and characteristics of traffic jams, *Phys. Rev. E* **53**, R1297(R) (1996).
- [34] EV-Database, <https://ev-database.org/cheatsheet/range-electric-car>.
- [35] C. Hecht, S. Das, C. Bussar, and D. U. Sauer, Representative, empirical, real-world charging station usage characteristics and data in Germany, *eTransportation* **6**, 100079 (2020).
- [36] Tesla Supercharger, <https://www.tesla.com/supercharger>.
- [37] R. Bennett, Queues, customer characteristics and policies for managing waiting-lines in supermarkets, *Int. J. Retail Distrib. Manag.* **26**, 78 (1998).
- [38] P. L. Krapivsky and S. Redner, Simple parking strategies, *J. Stat. Mech. Theory Exp.* (2019) 093404.
- [39] Vehicles have a typical velocity of $v_0 = 120\text{km/h}$, a maximum range of $q_{\text{max}} = 300\text{km}$, and a charging threshold $q^* = 150\text{km}$. A charging station with four charging points and charging speeds of $\xi = 480\text{km/h}$ each is located equidistantly every $\ell = 15\text{km}$. The critical inflow rate is $\lambda_c = 256\text{veh/h}$. Simulated inflow rates are $\lambda_1 = 150\text{veh/h}$ in panel (a), $\lambda_2 = 300\text{veh/h}$ in panel (b), and $\lambda_3 = 230\text{veh/h}$ in panel (c). Reasoning and in-depth estimation of parameters can be found in the Supplemental Material.
- [40] S. Maerivoet and B. De Moor, Non-concave fundamental diagrams and phase transitions in a stochastic traffic cellular automaton, *Eur. Phys. J. B* **42**, 131 (2004).

- [41] A. Pottmeier, R. Barlovic, W. Knospe, A. Schadschneider, and M. Schreckenberg, Localized defects in a cellular automaton model for traffic flow with phase separation, *Physica A (Amsterdam, Neth.)* **308**, 471 (2002).
- [42] J. Sethna, *Statistical Mechanics: Entropy, Order Parameters, and Complexity* (Oxford University Press, New York, 2021), Vol. 14.
- [43] Y. Holovatch, R. Kenna, and S. Thurner, Complex systems: physics beyond physics, *Eur. J. Phys.* **38**, 023002 (2017).
- [44] C. Castellano, S. Fortunato, and V. Loreto, Statistical physics of social dynamics, *Rev. Mod. Phys.* **81**, 591 (2009).
- [45] SimPy, <https://gitlab.com/team-simpy/simpy/>.
- [46] OpenStreetMap, <https://www.openstreetmap.org>.
- [47] G. Boeing, OSMnx: New methods for acquiring, constructing, analyzing, and visualizing complex street networks, *Comput. Environ. Urban Syst.* **65**, 126 (2017).
- [48] Bundesnetzagentur, <https://www.bundesnetzagentur.de>.
- [49] K. Heineke, P. Kampshoff, M. Bertoncello, G. Camplone, A. Husain, P. Hertzke, M. Linder, S. Sahdev, B. Heid, M. Linder, M. Wilthaner, T. Baltic, R. Hensley, and J. Salazar, The Trends Transforming Mobility's fFuture, <https://www.mckinsey.com/industries/automotive-and-assembly/our-insights/the-trends-transforming-mobilitys-future#>.
- [50] Tesla Model S, <https://www.tesla.com/models>.
- [51] Bundesanstalt für Straßenwesen, <https://www.bast.de>.